Quantification of Surface Oxides on Carbonaceous Materials

Laura A. Langley,† Daniel E. Villanueva,† and D. Howard Fairbrother*,†,‡

Departments of Chemistry and Materials Science and Engineering, Johns Hopkins University, 3400 North Charles Street, Baltimore, Maryland 21218

Received July 6, 2005. Revised Manuscript Received October 3, 2005

X-ray photoelectron spectroscopy (XPS) in conjunction with chemical derivatization has been developed to quantify the concentrations of hydroxyl, carboxylic acid, and carbonyl groups on carbonaceous surfaces, specifically black carbons (BCs). Control studies on polymers and graphite were performed to establish the selectivity and stoichiometry of each derivatization reaction toward the targeted oxide. Hydroxyl groups were successfully derivatized with trifluoroacetic anhydride. Derivatization strategies using trifluoroethanol, however, had to be modified from protocols used in polymer studies in order to effectively derivatize carboxylic acid groups on BCs. Derivatizing agents previously used to target carbonyl groups on polymers were found unsuitable for BC materials because of nonspecific adsorption interactions between the phenyl ring of the derivatizing agent and the extended graphene sheets of the BCs. These complications were overcome by employing trifluoroethyl hydrazine as a new derivatizing agent for the quantification of carbonyl groups. These three derivatization reactions were used in combination with XPS to quantify the surface concentrations of hydroxyl, carboxylic acid, and carbonyl groups on several BC materials including natural chars, soots, and an activated carbon. Experiments using these derivatization reactions in conjunction with energy dispersive spectroscopy were also evaluated as a means to probe the oxide concentrations within the bulk of these materials.

I. Introduction

Carbonaceous materials are used in an increasing number of technologically important applications. Examples include carbon nanotubes and sputter-deposited carbonaceous thin films. The surfaces of these materials are typically decorated with a variety of different oxides whose presence has a significant impact on their chemical properties. For example, the surface oxides on carbon nanotubes govern both their sorption and solubility properties.[1−5] Similarly, both the adhesion and friction properties of sputter-deposited amorphous carbon films are influenced by the presence of surface oxides.[6,7]

Another important class of carbonaceous materials are black carbons (BCs). These materials are formed as a result of the incomplete combustion of biomass or fuel sources. Wood chars and soot are naturally occurring forms of BC found in the environment, while activated carbons are examples of BCs manufactured synthetically for remediation strategies. All BCs have high surface areas, making them effective sorbents of a variety of chemicals. The sorption properties of BC materials are determined by a complex combination of both physical and chemical characteristics.[8−16] Relevant physical properties of BC materials include surface area and microporosity. The chemical characteristics of BCs are strongly influenced by the presence of heteroatoms. Oxygen is the most common heteroatom in BCs and is present in a wide variety of oxygen-containing functional groups or surface oxides. As shown by Figure 1, the surface oxides on BCs decorate the edges of individual graphene sheets, which are themselves a characteristic feature of all BCs. Figure 1 also shows that the surface oxides on BCs exist in a variety of oxygen-containing functional groups that include, but are not limited to, carboxylic acid, phenolic, hydroxyl, carbonyl, lactone, pyrone, and anhydride functionalities.[13,17−24]

* Corresponding author. E-mail: howardf@jhu.edu. Phone: (410)516-4328. Fax: (410)516-8420.
† Department of Chemistry.
‡ Department of Materials Science and Engineering.

(1) Ellison, M. D.; Good, A. P.; Kinnaman, C. S.; Padgett, N. E. *J. Phys. Chem.* **2005**, *109*, 10640.
(2) Kuznetsova, A.; Popova, I.; Yates, J. T.; Bronikowski, M. J.; Huffman, C. B.; Liu, J.; Smalley, R. E.; Hwu, H. H.; Chen, J. G. *J. Am. Chem. Soc.* **2001**, *123*, 10699.
(3) Banerjee, S.; Wong, S. S. *J. Phys. Chem. B* **2002**, *106*, 12144.
(4) Feng, X.; Matranga, C.; Vidic, R.; Borguet, E. *J. Phys. Chem. B* **2004**, *108*, 19949.
(5) Xing, Y.; Li, L.; Chusuei, C. C.; Hull, R. V. *Langmuir* **2005**, *21*, 4185.
(6) Voevodin, A. A.; O'Neill, J. P.; Zabinski, J. S. *Thin Solid Films* **1999**, *342*, 233.
(7) Fontaine, J.; Le Mogne, T.; Loubet, J. L.; Belin, M. *Thin Solid Films* **2005**, *482*, 99.
(8) Jiang, Z. X.; Liu, Y.; Sun, X. P.; Tian, F. P.; Sun, F. X.; Liang, C. H.; You, W. S.; Han, C. R.; Li, C. *Langmuir* **2003**, *19*, 731.
(9) Rangel-Mendez, J. R.; Streat, M. *Water Res.* **2002**, *36*, 1244.
(10) Moreno-Castilla, C.; Lopez-Ramon, M. V.; Carrasco-Marin, F. *Carbon* **2000**, *38*, 1995.
(11) Figueiredo, J. L.; Pereira, M. F. R.; Freitas, M. M. A.; Orfao, J. J. M. *Carbon* **1999**, *37*, 1379.
(12) Li, L.; Quinlivan, P. A.; Knappe, D. R. U. *Carbon* **2003**, *41*, 1693.
(13) Chen, J. P.; Wu, S. N. *Langmuir* **2004**, *20*, 2233.
(14) Braida, W. J.; Pignatello, J. J.; Lu, Y. F.; Ravikovitch, P. I.; Neimark, A. V.; Xing, B. S. *Environ. Sci. Technol.* **2003**, *37*, 409.
(15) Hong, L.; Ghosh, U.; Mahajan, T.; Zare, R. N.; Luthy, R. G. *Environ. Sci. Technol.* **2003**, *37*, 3625.
(16) Nguyen, T. H.; Sabbah, I.; Ball, W. P. *Environ. Sci. Technol.* **2004**, *38*, 5488.
(17) Akhter, M. S.; Chughtai, A. R.; Smith, D. M. *Appl. Spectrosc.* **1991**, *45*, 653.
(18) Akhter, M. S.; Chughtai, A. R.; Smith, D. M. *Appl. Spectrosc.* **1985**, *39*, 143.

10.1021/cm051462k CCC: $33.50
Published on Web 12/13/2005

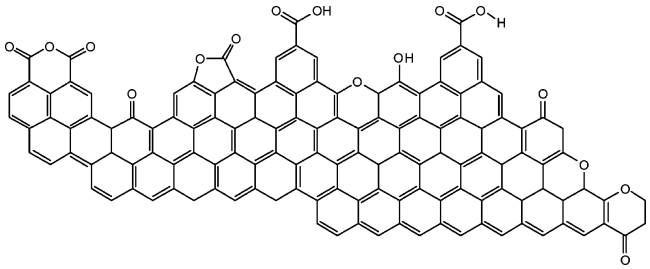

Figure 1. Representative structure of an individual graphene sheet in a BC material, indicating the range of surface oxides present. Functional groups present include anhydrides, ketones, lactones, carboxylic acids, ethers, hydroxyls, and pyrones.

An array of analytical methods has been used to characterize the oxides on BCs. Among these techniques, infrared (IR) spectroscopies have been one of the most widely used,[17,18,21,23−27] although temperature-programmed desorption (TPD)[23,28−31] and Boehm titrations[8,19,23] have also been employed. Information obtained from these techniques has provided valuable insights into the chemical composition of BC materials, including the identification of the functional groups shown in Figure 1. However, only limited quantitative information on the concentration of the oxides can be obtained from these techniques. For example, IR studies are hindered by difficulties in accurately assigning IR bands, as well as the inability to obtain quantitative information on oxide concentrations. Similarly, analysis of TPD data is often ambiguous due to the fact that multiple oxides decompose at similar temperatures and give rise to similar decomposition products, such as CO, CO_2, and H_2O. Boehm titrations have also been used to quantify the pK_a ranges existing within a BC material, but do not provide quantitative information on the concentration of different surface oxides.

In contrast to the techniques discussed above, XPS is an analytical technique that can provide quantitative information on the oxides present on the surface of BC materials.[9,10,13,23,32] In addition to surface elemental composition, XPS can in principle also be used to determine the local bonding environments of C atoms. This is accomplished by fitting the C(1s) spectral envelope to include contributions from different surface oxides (e.g., *C*−O, *C*═O, O−*C*═O), each of which have peaks at different binding energies.[23,33] A number of studies have employed this type of spectral deconvolution in an attempt to quantify the distribution of surface oxides on BC and BC-like materials.[9,10,13,23,32] Spectral deconvolution of XPS peaks in the C(1s) region is, however, fraught with difficulty due to the close proximity of the binding energies associated with the different oxides and the limited resolution of typical XP spectrometers.[11,23,33] As a result, obtaining information on the concentrations and distributions of oxides on BCs is not possible using XPS in isolation.

In previous studies on modified polymer surfaces, derivatization reactions that target specific functional groups, have been developed and used in conjunction with XPS to provide information on the concentration and distribution of surface oxides.[34−40] For example, Chilkoti et al. used chemical derivatization in conjunction with XPS to examine the hydroxyl and carbonyl functional group distribution on plasma-deposited polymeric films.[37] Another study by Popat et al. employed chemical derivatization to determine the distribution of hydroxyl and carboxylic acid groups produced during flame treatment of polypropylene surfaces.[36] Chemical derivatization combined with XPS has also been used to determine the concentration of surface oxides on carbon fibers.[35,41,42] The chemicals used to target these oxides are referred to as derivatizing agents and contain a chemically distinct tag. When chemical derivatization is used in conjunction with XPS, the fluorine atoms in a CF_3 group are often used as the chemical tag. This is due to the fact that fluorine is absent from the native surface of most materials, including BCs. In addition, fluorine also has a high cross section for detection by XPS, improving the sensitivity of the derivatization reaction. Derivatization strategies can also distinguish between certain oxides that are contained within the same XPS peak component. For example, both hydroxyl (C−OH) and ether (C−O−C) functional groups are peak fit in the same C−O component using conventional XPS peak fitting methods; however, hydroxyl groups can be specifically targeted using derivatization reactions. Another derivatization approach has recently been developed, which uses fluorescent chromophores as labels to measure the concentrations of hydroxyl, carboxylic acid, and carbonyl groups on self-assembled monolayer surfaces.[43] This technique can quantify these oxides at extremely low concentrations (0.01−10% of a monolayer).

(19) Lopez-Garzon, F. J.; Domingo-Garcia, M.; Perez-Mendoza, M.; Alvarez, P. M.; Gomez-Serrano, V. *Langmuir* **2003**, *19*, 2838.
(20) Beck, N. V.; Meech, S. E.; Norman, P. R.; Pears, L. A. *Carbon* **2002**, *40*, 531.
(21) Smith, D. M.; Chughtai, A. R. *Colloids Surf. A* **1995**, *105*, 47.
(22) Blom, L.; Edelhausen, L.; Vankrevelen, D. W. *Fuel* **1957**, *36*, 135.
(23) Boehm, H. P. *Carbon* **2002**, *40*, 145.
(24) Fuente, E.; Menendez, J. A.; Suarez, D.; Montes-Moran, M. A. *Langmuir* **2003**, *19*, 3505.
(25) Fuente, E.; Menendez, J. A.; Diez, M. A.; Suarez, D.; Montes-Moran, M. A. *J. Phys. Chem. B* **2003**, *107*, 6350.
(26) Fanning, P. E.; Vannice, M. A. *Carbon* **1993**, *31*, 721.
(27) Smith, D. M.; Keifer, J. R.; Novicky, M.; Chughtai, A. R. *Appl. Spectrosc.* **1989**, *43*, 103.
(28) Szymanski, G. S.; Karpinski, Z.; Biniak, S.; Swiatkowski, A. *Carbon* **2002**, *40*, 2627.
(29) Raymundo-Pinero, E.; Cazorla-Amoros, D.; Linares-Solano, A. *Carbon* **2001**, *39*, 231.
(30) Haydar, S.; Moreno-Castilla, C.; Ferro-Garcia, M. A.; Carrasco-Marin, F.; Rivera-Utrilla, J.; Perrard, A.; Joly, J. P. *Carbon* **2000**, *38*, 1297.
(31) Zhuang, Q. L.; Kyotani, T.; Tomita, A. *Energy Fuels* **1994**, *8*, 714.
(32) Valdes, H.; Sanchez-Polo, M.; Rivera-Utrilla, J.; Zaror, C. A. *Langmuir* **2002**, *18*, 2111.
(33) Vickerman, J. C. *Surface Analysis: The Principal Techniques*; John Wiley & Sons Ltd.: West Sussex, 1997.
(34) Chevallier, P.; Castonguay, N.; Turgeon, S.; Dubrulle, N.; Mantovani, D.; McBreen, P. H.; Wittmann, J. C.; Laroche, G. *J. Phys. Chem. B* **2001**, *105*, 12490.
(35) Povstugar, V. I.; Mikhailova, S. S.; Shakov, A. A. *J. Anal. Chem.* **2000**, *55*, 405.
(36) Popat, R. P.; Sutherland, I.; Sheng, E. S. *J. Mater. Chem.* **1995**, *5*, 713.
(37) Chilkoti, A.; Ratner, B. D.; Briggs, D. *Chem. Mater.* **1991**, *3*, 51.
(38) Batich, C. D. *Appl. Surf. Sci.* **1988**, *32*, 57.
(39) Gerenser, L. J.; Elman, J. F.; Mason, M. G.; Pochan, J. M. *Polymer* **1985**, *26*, 1162.
(40) Sutherland, I.; Sheng, E.; Brewis, D. M.; Heath, R. J. *J. Mater. Chem.* **1994**, *4*, 683.
(41) Alexander, M. R.; Jones, F. R. *Carbon* **1995**, *33*, 569.
(42) Yin, M.; Koutsky, J. A.; Barr, T. L.; Rodriguez, N. M.; Baker, R. T. K.; Klebanov, L. *Chem. Mater.* **1993**, *5*, 1024.
(43) McArthur, E. A.; Ye, T.; Cross, J. P.; Petoud, S.; Borguet, E. *J. Am. Chem. Soc.* **2004**, *126*, 2260.

Table 1. Polymers Used for Controls Studies along with Their Preparation Conditions

polymer	monomer unit	functional group[a]	casting solution
poly(*p*-hydroxystyrene) (PHS)	$[CH_2CH(C_6H_4OH)]_n$	hydroxyl(Ph)	4% w/v in 1,4-dioxane
poly(vinyl alcohol) (PVA)	$[CH_2CH(OH)]_n$	hydroxyl	2% w/v in MilliQ water
poly(*p*-benzoic acid) (PBA)	$[CH_2CH(C_6H_4COOH)]_n$	carboxylic acid (Ph)	2% w/v in THF
poly(acrylic acid) (PAA)	$[CH_2CH(CO_2H)]_n$	carboxylic acid	2% w/v in methanol
poly(vinyl methyl ketone) (PVMK)	$[CH_2CH(COCH_3)]_n$	ketone	1% w/v in chloroform
poly(methyl methacrylate) (PMMA)	$[CH_2C(CH_3)(CO_2CH_3)]_n$	ester	3% w/v in chloroform
poly(ethylene terephthalate) (PET)	$[O(CH_2)_2O_2C(C_6H_4)CO]_n$	ester(Ph)	n/a
poly(ethylene oxide) (PEO)	$[CH_2CH_2O]_n$	ether	2% w/v in chloroform

[a] Ph denotes that the functional group listed is attached to a phenyl ring.

In this paper, we describe an important extension of chemical derivatization used in conjunction with XPS, developed specifically to quantify the concentration of several key surface oxides on BCs, namely, hydroxyl, carboxylic acid, and carbonyl groups. Each derivatization reaction has been carefully characterized in terms of its selectivity and overall reactivity using a suite of polymers, each containing a functional group that closely represents an individual oxide found on BCs. To address the possible interference with the graphene sheets of BC materials, the reactivity of each derivatizing agent with graphite has also been examined. The experimental methodology developed in this study has been applied to study the variability of surface oxides on a number of different BC materials.

II. Experimental Section

2.1. Materials. BC materials studied in this investigation consisted of three natural chars (NC1, NC2, and NC3), one diesel soot (DS), one hexane soot (HS), and one activated charcoal (AC). DS was a NIST standard reference material (SRM) 2975. HS was obtained from the laboratories of Dwight Smith at the University of Colorado. AC was purchased from Aldrich respectively, and used as received.

Natural char (NC) samples were taken from burnt logs of pitch pine (*Pinus rigida*) collected by hand from a prescribed burn site in the Lebanon State Forest of the New Jersey Pinelands (Burlington Co., NJ) in November 2000 (NC1 and NC2) and in April 2002 (NC3). The clearly charred portions were scraped from the logs. All NC samples were ground into a fine powder in a ball mill and sieved to isolate the fraction finer than 400 mesh ($\leq 38\ \mu$m). The ground and sieved material was carefully homogenized by end-over-end rotation for 24 h.[44]

Initial experiments revealed that calcium present in the natural chars (NCs) reacted with the fluorine-containing derivatizing reagents. This produced an exaggerated F(1s) XP signal and interfered with analysis of derivatized NC samples. As a result, homogenized NC samples were acid-washed to remove inorganic impurities, specifically calcium, prior to chemical derivatization. Acid washing was accomplished by submersing 1.5 g of NC in 250 mL of a 10% HCl solution (by volume). The acid solution was continuously stirred for 2 h and then filtered (Whatman glass microfiber, 1.5 μm), and the liquid was discarded. The filtered char was then added to a fresh 250 mL aliquot of 10% HCl and continuously stirred for an additional 2 h. The acid-washed char was filtered again and rinsed with MilliQ water until the pH of the filtrate was equal to the pH of the MilliQ water. It should be noted that although acid washing removed Ca, it did not change the overall O/C ratio or the XPS C(1s) and O(1s) line shapes of the native materials. In contrast to NCs, the hexane and diesel soot, and AC did not contain Ca, and therefore did not require acid washing.

Polymers were purchased commercially. Poly(ethylene terephthalate) (PET) was obtained from Goodfellow. Poly(vinyl alchol) (PVA), poly(acrylic acid) (PAA), poly(vinyl methyl ketone) (PVMK), poly(ethylene oxide) (PEO), and poly(*p*-hydroxystyrene) (PHS) were purchased from Aldrich. Poly(methyl methacrylate) (PMMA) was purchased from Alfa Aesar. Poly(benzoic acid) (PBA) was purchased from Polymer Source, Inc.

Highly ordered pyrolytic graphite (HOPG) was purchased from SPI Supplies. A clean HOPG surface was prepared before each derivatization reaction by peeling off the three topmost layers of HOPG with scotch tape.

Derivatizing agents, specifically trifluoroacetic anhydride (TFAA), trifluoroethanol (TFE), 1,3-di-*tert*-butyl-carbodiimide (DTBC), trifluoroethyl hydrazine (TFH), and trifluoromethyl phenyl hydrazine (TFMPH) were purchased from Aldrich and used as received. All reagents were 99% pure, with the exception of TFH, which was obtained as a 70% solution (by volume) in water. Phenyl trifluoroacetate (PTFA) was also purchased from Aldrich. Solvents used for cleaning and casting polymers, including toluene, ethanol, 1,4-dioxane, chloroform, methanol, tetrahydrofuran, and pyridine, were purchased from Fisher Chemicals.

2.2. Preparation of Polymer Surfaces. Polymers were spin cast onto PET substrates (4000 rpm, 30 s) using a Laurell Tech Corporation spin coater (Model #WS-400A-6NP/LITE). Prior to casting, PET surfaces were cleaned by ultrasonification in toluene and ethanol solutions. XPS analysis was used to determine the quality of each spin-cast polymer surface. Detailed XPS analyses of the polymer films were performed by peak fitting (70% Gaussian/30% Lorentzian) the C(1s) and O(1s) regions using CASA XPS software. Details of casting solutions are given in Table 1, along with the names, abbreviations, and monomer units of each polymer.

2.3. XPS Analysis. Prior to XPS analysis, polymer samples were mounted onto standard sample stubs and secured by washers. BC samples were sprinkled onto copper tape (3M). The absence of any copper signal was used to ensure that the BC sample completely covered the adhesive and that the adhesive tape did not contribute to the overall XPS signal.

XPS analysis of polymer films and BC samples was carried out in an ultra-high-vacuum chamber equipped with a fast-entry introductory chamber. Prior to analysis, all samples were evacuated in the introductory chamber using a turbo-molecular pump for at least 90 min to ensure removal of all volatile species from the BC or polymer substrate. Samples were then introduced into the XPS analysis chamber ($P_{base} \approx 1 \times 10^{-8}$ Torr). XP spectra were recorded using the X-ray irradiation from a Mg Kα anode from a Physical Electronics 04-500 dual-anode X-ray source and 10-360 precision energy analyzer. All XP spectra were acquired at 15 kV and 300 W. Elemental scans were acquired using a pass energy of 44.75 eV and a resolution of 0.125 eV/step. Binding energies were referenced to the CC/ CH_2 C(1s) peak at 284.6 eV.[45]

(44) Nguyen, T. H.; Brown, R. A.; Ball, W. P. *Org. Geochem.* **2004**, *35*, 217.

2.4. Attenuated Total Reflectance-Infrared (ATR-IR) Analysis. ATR-IR spectra were acquired with an attenuated total reflection device (Pike Technolgies MIRacle) equipped with a diamond crystal in single reflection mode using a Mattson Infinity Series FTIR spectrometer with a Mercury cadmium telluride detector (2 cm^{-1} resolution). Spectra for organic chemicals and BC materials represent an average of 500 and 2500 scans, respectively. All spectra were ratioed to Al foil.

2.5. Energy Dispersive Spectroscopy (EDS) Analysis. EDS was performed using a scanning electron microscope (JEOL 6700F) equipped with an Edax Genesis 4000 X-ray analysis system (detector resolution of 129 eV). All EDS measurements were taken in duplicate.

2.6. Chemical Derivatization. Vapor-phase chemical derivatization of BC and polymer samples was carried out in a custom-made glass reaction vessel, designed to keep the derivatizing agent and the sample in close spatial proximity (<2 in.) while preventing them from coming into physical contact (a schematic of this reaction vessel is shown in Supporting Information Figure 1). This was done to minimize any potential changes in the materials being derivatized, as well as to eliminate any sorption and/or surface swelling effects due to the physical interactions between the liquid-phase derivatizing agents and the samples. In addition, the close proximity of the derivatizing agent and the sample improved the efficiency of the derivatization reactions compared to the same reactions carried out with the sample and derivatizing agent in separate reaction vessels.

Derivatization experiments are initiated by placing the sample and derivatizing agent in the reaction vessel. The derivatizing agent is then frozen with liquid nitrogen, and the reaction vessel is pumped down to approximately 50 mTorr using a mechanical pump. The reaction vessel is then sealed using a stopcock and allowed to warm to room temperature under low vacuum, thereby initiating vapor phase reaction between the derivatizing agent and the substrate.

Derivatization procedures varied slightly for each reaction. Hydroxyl groups were derivatized using 1 mL of TFAA. The derivatization of carboxylic acid groups was accomplished using a mixture of TFE (1.1 mL), pyridine (0.4 mL), and DTBC (1.0 mL). Carbonyl groups were derivatized using either 1 mL of TFMPH or TFH. In experiments using TFMPH, the reagent was kept at a constant temperature of 65 °C with a mineral oil bath due to its low vapor pressure at room temperature. Carbonyl groups were also derivatized with TFH. In contrast to the derivatization of carbonyl groups with TFMPH, this reaction did not require heating.

Derivatization reactions with both polymer and BC samples were assumed to have reached completion when additional reaction time did not result in any increase in the F(1s) signal, measured by XPS. A total reaction time of 4 h was found to be sufficient to complete reactions on polymer surfaces. For BC samples, however, 15 h was necessary to ensure complete reaction (see Supporting Information Figure 2 for uptake curve). For XPS analysis 5−10 replicates were taken for each derivatized BC material over a period of 15−40 h of total reaction time. The error associated with each measurement was based on the standard deviation obtained from XPS analysis of these 5−10 replicates. In each case the measured error was no greater than 10% of the reported value. Furthermore, the overall reproducibility of the experimental procedure is supported by the fact that separate derivatizing experiments carried out on the same polymer substrate yielded identical XPS results (±1%).

The stability of the fluorine-containing surface products toward X-rays was assessed by exposing derivatized polymer and BC samples to prolonged irradiation (2 h). XPS analysis before and after X-ray irradiation showed that the concentration of fluorine did not change. As a result, it was concluded that the surface composition was not influenced by X-ray irradiation during sample analysis (≈30 min).

III. Results and Discussion

3.1. Derivatization of Control Surfaces. Control studies on well-characterized polymer surfaces and HOPG were performed to assess the selectivity and stoichiometry of each derivatization reaction. Table 1 lists the names, functional groups, and monomer units of the polymers used for these control studies. The cleanliness of the native polymer surfaces was verified by XPS analysis. Results from these analyses are given in the Supporting Information (SI Figure 3). Wherever possible, both aromatic and aliphatic polymers containing oxide functional groups that are representative of surface oxides encountered on BC materials were used. For example, PET is used to model ester functional groups on BC materials and also serves as a model for lactones (cyclic esters). HOPG was used as a control to model the graphene sheets, which are an integral component of all BCs.

Additional experiments were attempted using model compounds, such as naphthoflavone, to represent other, more complex oxides such as quinones and pyrones also present on BC surfaces. However, clean, stoichiometric surfaces of these model compounds could not be prepared either from the as-received powder or from solutions of the compounds spin-coated onto PET substrates. For this reason, these compounds were not used as models for BC surface oxides in the derivatization experiments discussed below.

3.1.1. Derivatization of Hydroxyl Groups. Previous studies on the vapor-phase derivatization of polymer surfaces have established that TFAA undergoes an esterification reaction with surface hydroxyl (−OH) groups as shown in reaction 1.[36,37,46] However, few studies have examined the selectivity

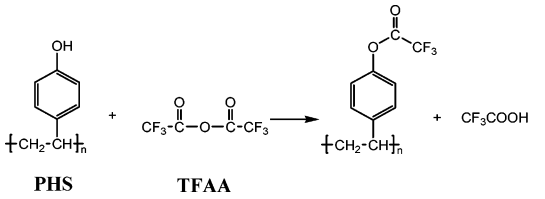

(1)

and stoichiometry of TFAA toward aromatic polymers containing hydroxyl groups (e.g. PHS), which are more representative of those present on BCs (reaction (1)).[37] Figure 2 shows the F(1s) XP signal observed on each of the polymer surfaces listed in Table 1, and graphite, after exposure to TFAA. The large F(1s) signals observed on PHS and PVA, in combination with the much smaller F(1s) signals observed on the other polymer surfaces, demonstrates that TFAA reacts selectively with hydroxyl groups.

After reaction with TFAA, the atomic percentage of fluorine on a surface containing hydroxyl groups can be calculated using eq 2,[36,40]

$$\%F = ((3\epsilon[O_0]_{OH})/([C_0] + [O_0] + 6\epsilon[O_0]_{OH})) \times 100 \qquad (2)$$

(45) Wagner, C. D.; Riggs, W. M.; Davis, L. E.; Moulder, J. F.; Muilenberg, G. E. *Handbook of X-Ray Photoelectron Spectroscopy*; Perkin-Elmer Corporaion: Eden Prairie, MN, 1979.

(46) Ameen, A. P.; Ward, R. J.; Short, R. D.; Beamson, G.; Briggs, D. *Polymer* **1993**, *34*, 1795.

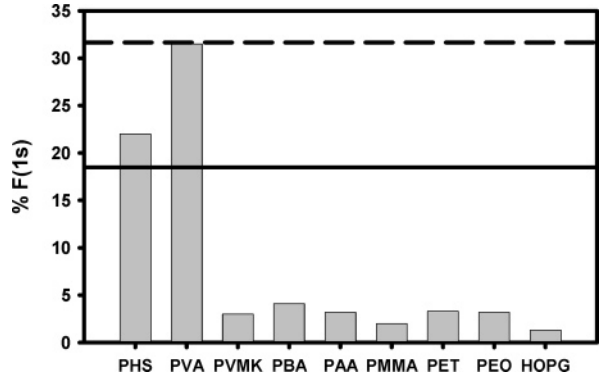

Figure 2. F(1s) XP signal detected on each polymer surface, and HOPG, after reaction with TFAA. Lines indicate the percentage of fluorine predicted on the hydroxyl-containing polymers, PHS (solid line) and PVA (dashed line), after derivatization with TFAA assuming 100% reaction efficiency.

In this equation $[C_0]$ and $[O_0]$ are the initial concentrations of C and O present on the surface (determined by XPS), and $[O_0]_{OH}$ is the surface concentration of hydroxyl groups. In the case of PHS and PVA, $[O_0]_{OH}$ is equal to $[O_0]$. The efficiency of the reaction is given by ϵ, which is equal to 1 if all of the hydroxyl groups on the surface react with TFAA, and 0 if no reaction occurs. Equation 2 was derived from the stoichiometry of reaction 1. Thus by using eq 2, the percentage of fluorine on a derivatized surface with a known concentration of hydroxyl groups (such as PHS or PVA) can be calculated. Equation 2 can also be rearranged to give eq 3,[36,40]

$$\%\,[O_0]_{OH} = ([F][C_0] + [F][O_0])/(3\epsilon - 6\epsilon[F]) \times 100 \qquad (3)$$

This expression is useful for determining $[O_0]_{OH}$ on BC materials, where multiple types of oxides are present and the concentration of hydroxyl groups is unknown.

The solid and dashed lines in Figure 2 represent the concentration of fluorine predicted on the surfaces of PHS and PVA, respectively, if the esterification reaction with TFAA proceeded with 100% efficiency (i.e., $\epsilon = 1$ in reaction 2). The close proximity of the predicted values (lines) and experimental measurements (bars) indicates that TFAA reacts with all of the surface hydroxyl groups on PHS and PVA.

Information on the efficiency of the derivatization reaction shown in reaction 1 can also be obtained from peak fitting the C(1s), O(1s), and F(1s) XPS regions of PHS before (Figure 3a) and after (Figure 3b) esterification with TFAA. In addition to the appearance of a F(1s) signal in Figure 3b, both the C(1s) and O(1s) regions are modified by the reaction of TFAA with PHS. Before derivatization, there are two major peaks in the C(1s) region, corresponding to *C*−C and *C*−O species, along with a much weaker $\pi-\pi^*$ shake up feature at higher binding energies. After derivatization, the C(1s) region can be well-fit with four major peaks, corresponding to *C*−C, *C*−O, O−*C*═O, and *C*F_3 species, along with a minor contribution from the $\pi-\pi^*$ shake-up feature. Based on the integrated XPS peak areas, the ratio of the *C*−C:*C*−O:*C*(O)O:*C*F_3 species is 8:1:1:1, which is very close to the calculated theoretical ratio of 7:1:1:1. The slight overrepresentation of the *C*−C peak is most likely due to the presence of a small amount of adventitious carbon on the surface. After derivatization the area under the *C*F_3 component is 11% of the total area within the C(1s) region. This agrees favorably with the predicted value of 10% calculated based on reaction 1.

The O(1s) region in Figure 3 also changes significantly after derivatization of PHS with TFAA. Initially, there is only one peak due to the −*O*H oxygen species. After derivatization, the O(1s) spectral envelope can be well-fit by two peaks of equal magnitude. These two peaks correspond to the two different types of oxygen in the ester surface product, *O*−C and *O*═C. Although the results are not presented here, a similar analysis of the C(1s), O(1s), and F(1s) regions of PVA before and after reaction with TFAA was also performed; the results of this analysis indicate that this reaction also proceeds with 100% efficiency.

3.1.2. Derivatization of Carboxylic Acid Groups. Carboxylic acids, such as those on PBA, were derivatized using TFE (reaction 4). This reaction proceeds via a dicyclohexylcarbodiimide (DCC) peptide coupling mechanism, which requires the presence of DTBC (an imide) and pyridine.[47]

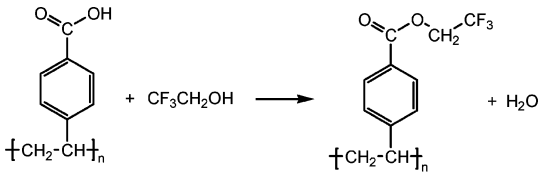

(4)

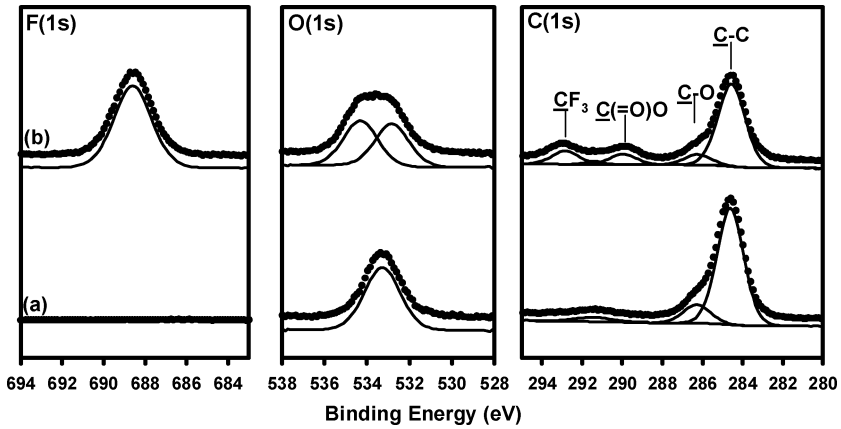

Figure 3. F(1s), O(1s), and C(1s) XP spectral regions of PHS before (a) and after (b) derivatization with TFAA.

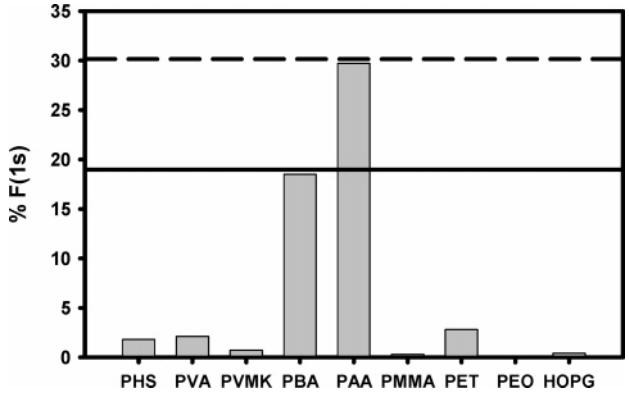

Figure 4. F(1s) XP signal detected on each polymer surface, and HOPG, after derivatization with TFE. Lines indicate the percentage of fluorine predicted on the carboxylic acid containing polymer surfaces, PBA (solid line) and PAA (dashed line), after derivatization with TFE assuming 100% reaction efficiency.

Previous studies have employed this reaction to derivatize carboxylic acid groups on aliphatic polymer surfaces, such as PAA, by using TFE, pyridine, and DTBC in a volume ratio of 9:4:3, respectively. In the present investigation 100% of the carboxylic acid groups on PAA were derivatized using this volume ratio. However, only 50% of the carboxylic acid groups on PBA were derivatized using the same reaction conditions. This difference in reactivity is attributed to the weaker acidity of the carboxylic acid proton on PBA compared to aliphatic analogues, such as PAA. Both PBA and PAA reacted to 100% completion with TFE when the volume of the imide (DTBC) was increased. The optimal ratio for TFE, pyridine, and DTBC was determined to be 11:4:10, respectively.

Figure 4 shows the reactivity of each of the polymers and graphite toward TFE, as determined from the F(1s) XP signal. The selectivity of this reaction toward carboxylic acid groups is confirmed by the large fluorine signals observed on both PBA and PAA, in addition to the absence of any appreciable fluorine uptake on the other substrates.

The surface concentration of carboxylic acid groups can be determined using a similar approach used for the quantification of hydroxyl groups. Based on the stoichiometry of reaction 4, the fluorine signal observed after derivatization of surface carboxylic acid groups can be calculated from eq 5,

$$\%F = ((3/2\epsilon[O_0]_{COOH})/([C_0] + [O_0] + 5/2\epsilon[O_0]_{COOH})) \times 100 \quad (5)$$

In this expression, $[C_0]$ and $[O_0]$ are the initial concentrations of C and O present on the surface as determined by XPS and $[O_0]_{COOH}$ is the surface concentration of carboxylic acid groups. In the case of PBA and PAA, $[O_0]_{COOH}$ is equal to $[O_0]$. Equation 5 is derived from reaction 4 in a similar manner as eq 2 except for the fact that three fluorine atoms are detected for the two oxygen atoms in each carboxylic acid group. Equation 5 can also be rearranged to give eq 6

$$\%\,[O_0]_{COOH} = ([F][C_0] + [F][O_0])/(3/2\epsilon - 5/2\epsilon[F]) \times 100 \quad (6)$$

This equation can be used to determine the concentration of carboxylic acid groups on a heterogeneous BC surface containing a mixture of different oxygen-containing functionalities.

The solid and dashed lines in Figure 4 indicate the theoretical values of fluorine expected on the surfaces of PBA and PAA, respectively, if reaction 4 proceeds with 100% efficiency (value calculated from eq 5 when $\epsilon = 1$). The close proximity of the predicted values (lines) and experimental measurements (bars) indicates that TFE reacts with all of the carboxylic groups on the surface of PBA and PAA.

XPS analysis of the C(1s), O(1s), and F(1s) regions of PBA before and after derivatization with TFE also support the idea of a stoichiometric reaction. Peak deconvolution of the C(1s) region of PBA after reaction with TFE reveals that the CF_3 component represents 8.2% of the total C(1s) region (see Supporting Information Figure 4 for spectra and peak fits). This value is close to the theoretical value of 9.0%, calculated on the basis of the surface product shown in reaction 4. A similar analysis conducted on PAA reveals that the derivatization of aliphatic carboxylic acids using TFE also proceeded with approximately 100% efficiency.

3.1.3. Derivatization of Carbonyl Groups. Fluorinated derivatives of hydrazines, such as TFMPH and pentafluorophenyl hydrazine (PFPH), have been used in previous studies to derivatize carbonyl groups on polymer surfaces.[35,36,38,48] In this study TFMPH was used to derivatize carbonyl groups on PVMK (reaction 7). TFMPH was

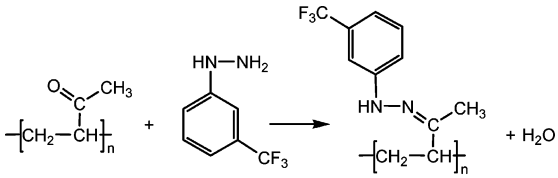

(7)

preferred over PFPH due to the fact that PFPH is a solid at room temperature.

Figure 5a shows the F(1s) XP signal on each polymer surface after derivatization with TFMPH. As expected, the largest uptake of fluorine occurs on PVMK. However, significant amounts of fluorine (>5%) are also observed on the surfaces of PET, PMMA, and HOPG after exposure to TFMPH. This is believed to be a result of $\pi-\pi$ interactions between the phenyl ring of TFMPH and the delocalized π electron systems on these three surfaces. Due to the presence of graphene sheets in BC materials (see Figure 1), a similar $\pi-\pi$ interaction is also expected to occur upon derivatization of BC samples with TFMPH (or PFPH). Thus, in contrast to previous studies on polymer surfaces, TFMPH cannot be used to derivatize carbonyl groups on BC materials. Similarly, the selectivity of fluorescent labeling techniques would likely be compromised by similar nonspecific $\pi-\pi$ bonding interactions between BC materials and the highly conjugated aromatic chromophores used as fluorescent reagents.[43]

(47) McMurry, J. *Organic Chemistry*, 2nd ed.; Brooks/Cole Publishing Company: Pacific Grove, CA, 1988.

(48) Zeggane, S.; Delamar, M. *Appl. Surf. Sci.* **1988**, *31*, 151.

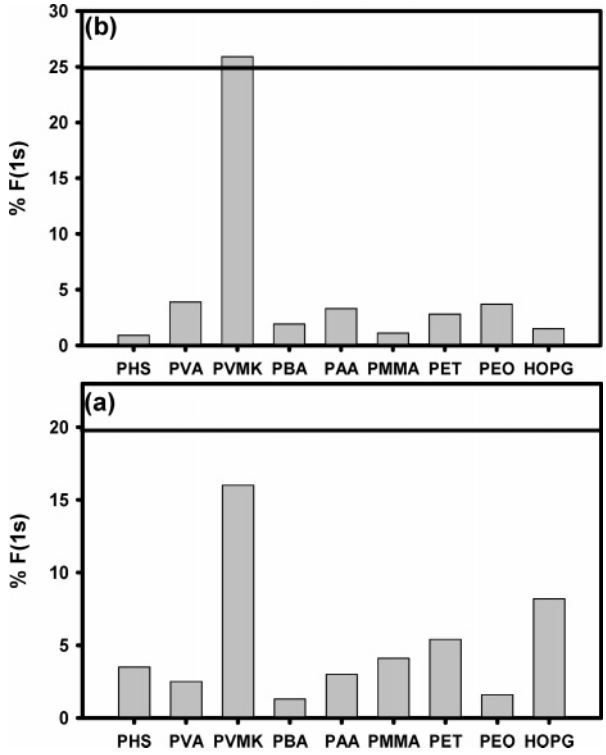

Figure 5. F(1s) XP signal detected on each polymer surface and HOPG after derivatization with TFMPH (a) and TFH (b). The solid lines indicate the percentage of fluorine predicted on the carbonyl containing polymer surface, PVMK, after derivatization with both TFMPH and TFH assuming 100% reaction efficiency.

In an attempt to overcome these limitations, TFH was introduced as a derivatizing agent for carbonyl groups on BC materials (reaction 8). TFH lacks the delocalized

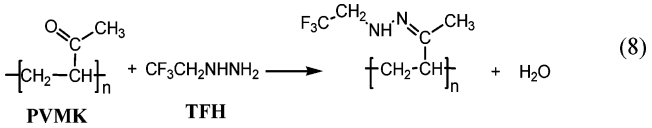

(8)

π-system found in TFMPH, but still contains the $-CF_3$ tag and reactive hydrazine functionality required for the derivatization of carbonyl groups. Figure 5b shows the F(1s) XP signal on each of the control surfaces after exposure to TFH. In contrast to TFMPH, TFH was found to be selective toward carbonyl groups based upon the significant fluorine uptake observed on PVMK in combination with the much smaller fluorine signals (<5%) observed on the other polymer surfaces and HOPG.

After derivatization with TFH, the F(1s) XPS signal on a surface containing carbonyl groups can be calculated from eq 9

$$\%F = ((3\epsilon[O_0]_{C=O})/([C_0] + [O_0] + 6\epsilon[O_0]_{C=O})) \times 100 \quad (9)$$

In this expression, $[C_0]$ and $[O_0]$ are the initial amounts of C and O present on the surface as determined by XPS, and $[O_0]_{C=O}$ is the surface concentration of carbonyl groups. For PVMK, $[O_0]_{C=O}$ is equal to $[O_0]$. Equation 9 can also be rewritten as

$$\%\,[O_0]_{C=O} = ([F][C_0] + [F][O_0])/(3\epsilon - 6\epsilon[F]) \times 100 \quad (10)$$

This expression can be used to calculate the surface concentration of carbonyl groups on materials containing a variety of different oxides (e.g., BC materials).

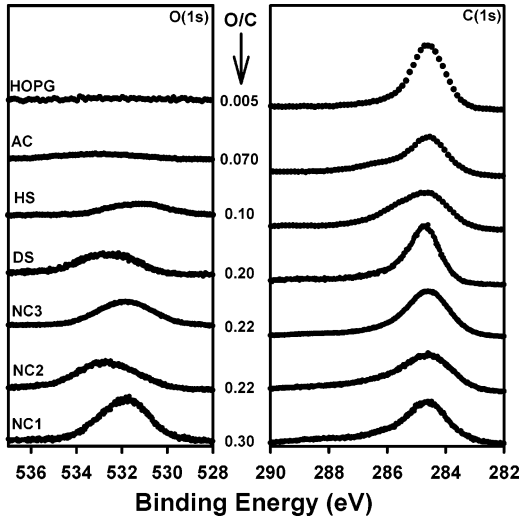

Figure 6. XP spectra of the O(1s) and normalized C(1s) regions for each BC material studied in this investigation. The ratio of the O(1s) peak area divided by the C(1s) peak area (O/C ratio) of each BC material is shown between the O(1s) and C(1s) regions.

The solid line in Figure 5b represents the predicted value of fluorine on the surface of PVMK if the reaction with TFH proceeds with 100% efficiency (value calculated from eq 9 when $\epsilon = 1$). The experimentally measured F(1s) intensity for PVMK (bar) is very close to the predicted value, indicating that the reaction between TFH and the carbonyl groups on PVMK is stoichiometric. Furthermore, a comparison of Figures 5a and 5b shows that the reaction of PVMK with TFH is more efficient (i.e., ϵ is closer to 1) than the reaction of PVMK with TFMPH.

Further evidence of the stoichiometry of reaction 8 can be obtained through analysis of the C(1s), O(1s), and F(1s) XPS regions before and after the derivatization of PVMK with TFH (spectra and peak fits are given in Supporting Information Figure 5). The *C*F_3 component comprises 14.5% of the total C(1s) area, which is very close to the theoretical atomic concentration of *C*F_3 (16.6%) found in the surface product shown in reaction 8. The loss of oxygen from the PVMK surface after exposure to TFH (from 20% O to 4% O) is further confirmation of a dehydration reaction. It should also be noted that TFH can only be obtained as a mixture containing 30% water; however, the presence of water does not appear to affect either the selectivity or stoichiometry of reaction 8.

In summary, the results presented in this section demonstrate that TFAA, TFE, and TFH react selectively with hydroxyl, carboxylic acid, and carbonyl groups, respectively. Furthermore, each of these three derivatizing reagents reacts with an extremely high efficiency ($\epsilon = 1$) toward the targeted surface oxide. These results support the idea that the concentration of hydroxyl, carboxylic acid, and carbonyl groups on BC materials can be determined using the derivatization reactions described in sections 3.1.1, 3.1.2, and 3.1.3, respectively.

3.2. XPS Analysis of Black Carbon Samples. The O(1s) and C(1s) XPS regions for each of the BC materials characterized in this investigation (including HOPG) are

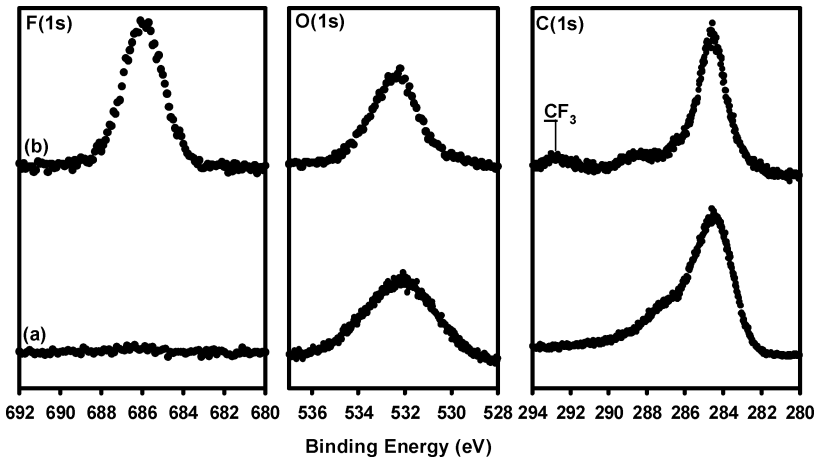

Figure 7. F(1s), O(1s), and C(1s) XP spectral regions of NC1 before (a) and after (b) derivatization with TFAA. The appearance of a CF_3 component in the C(1s) region after derivatization is evidence of the reaction between the reaction of hydroxyl groups on NC1 and TFAA.

shown in Figure 6. The ratio of the O(1s) peak area to the C(1s) peak area, or the O/C ratio (shown in the middle of Figure 6), provides a measure of the overall degree of oxidation of each BC material. Figure 6 shows that all of the BC materials are more oxidized than HOPG, and that there is significant variation in the degree of oxidation within the different BC materials. For example, NC1 has an O/C ratio of 0.30, while HS has a substantially lower level of oxidation (0.10).

In theory, it is possible to fit each of the C(1s) regions in Figure 6 with four major components (*C*−C, *C*−O, *C*═O, and O−*C*═O) to determine the distribution of surface oxides; however, in practice these regions can be equally well fit by a number of different variations of these four components. Thus, as discussed in the Introduction, peak fitting the C(1s) spectral envelope cannot be used to measure the distribution of surface oxides on BC materials. This has provided the motivation to apply chemical derivation strategies in conjunction with XPS to quantify the distribution of oxides on BC materials.

3.3. Derivatization of BCs. *3.3.1. XPS Analysis of Derivatized BC Materials.* Figure 7 shows the F(1s), O(1s), and C(1s) XPS regions of NC1 before (a) and after (b) derivatization of hydroxyl groups with TFAA. The observation of a F(1s) signal after derivatization is an indication of the reaction between the surface hydroxyl groups on NC1 and TFAA. Changes in the C(1s) region also suggest that a reaction with TFAA has occurred. Specifically, the appearance of intensities at higher binding energies in the C(1s) region (≅293 eV) denotes the presence of CF_3 species associated with the surface product (reaction 1).

Figure 8 shows the hydroxyl, carboxylic acid, and carbonyl concentrations measured on each BC material using the experimental protocols described in sections 2.4 and 3.1. These results are expressed as the percentage of the total BC surface occupied by each oxide (shaded regions) and are calculated using eqs 3, 6, and 10. The concentration of surface oxides not detected by any of the three derivatization reactions used in this study ("other oxides") is indicated by the unshaded portions of each bar in Figure 8. Thus, the total surface oxygen content on any BC material is given by the total height of each bar (sum of shaded plus unshaded regions). For example, Figure 8 shows that 63% of the total oxygen on NC1 is present as hydroxyl, carboxylic acid, or carbonyl groups and 37% of the total oxygen is distributed as "other" surface oxides. In contrast, on the AC surface the vast majority of the oxides are present on this surface as hydroxyl, carboxylic acid, or carbonyl groups while the concentration of "other" surface oxides is only 12%. These "other" oxides may exist as pyrones, lactones, ethers, esters, or anhydrides (see Figure 1).[8,13,18,21,23,49,50] These oxides are not targeted by the derivatization strategies employed in this investigation.

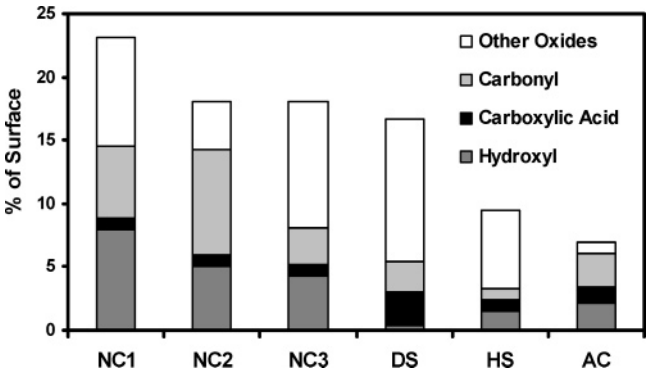

Figure 8. Percentage of hydroxyl, carboxylic acid, and carbonyl surface functional groups for each BC material. The surface concentration of each oxide was determined from separate derivatization experiments on each BC material. The unshaded regions of each bar indicate the percentage of surface oxides that were not identified by the derivatization reagents used in the present study (other oxides). The total height of the bar represents the total surface oxygen on each BC.

Figure 8 reveals similarities and differences in the distributions of hydroxyl, carbonyl, and carboxylic acid groups on the BC materials examined in this study. For example, NC1 and NC2 possess similar oxide distributions, with relatively high concentrations of hydroxyl and carbonyl groups, but significantly lower concentrations of carboxylic acid functionalities. The similar distribution of surface oxides is consistent with the fact that these two materials were collected at the same time and from locations close to one another. In contrast, the surface of NC3 possesses signifi-

(49) Sellitti, C.; Koenig, J. L.; Ishida, H. *Carbon* **1990**, *28*, 221.
(50) Domingo-Garcia, M.; Garzon, F. J. L.; Perez-Mendoza, M. J. *J. Colloid Interface Sci.* **2002**, *248*, 116.

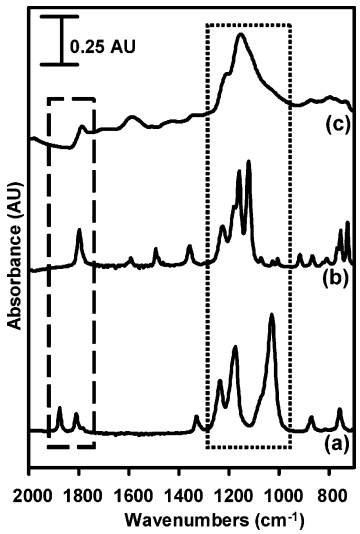

Figure 9. ATR-IR spectra of TFAA (a), PTFA (b), and NC1 after derivatization with TFAA (c). Dashed and dotted boxes show the C═O and C−F stretching regions, respectively.

cantly fewer carbonyl groups than either of the other two NC samples. This is most likely due to the fact that NC3 was collected from an annually burned site 2 years later than NC1 and NC2. Figure 8 also shows that diesel soot (DS) is distinctly different from all three natural chars, having a relatively large concentration of surface carboxylic acid and carbonyl groups, but very few hydroxyl groups. Diesel soot is the condensation product formed from the combustion of diesel fuel while the chars (NC1, NC2, and NC3) originate from the burning of pine wood; therefore, it is not surprising that the distribution of surface oxides on these BC materials differ significantly from each other.

3.3.2. ATR-IR Analysis of Derivatized BC Materials. To complement XPS analysis, ATR-IR spectroscopy has been used to study the reaction between TFAA and the hydroxyl groups on NC1. Figure 9 shows the ATR-IR spectra of (a) TFAA, (b) phenyl trifluoroacetate (PTFA), and (c) NC1 after exposure to TFAA. PTFA is used as a model compound for the ester surface product that is expected to form after the derivatization of hydroxyl groups with TFAA based on reaction 1.

A comparison of the carbonyl stretching regions in Figure 9 (dashed box) provides spectroscopic evidence for the specific reaction between TFAA and the hydroxyl groups on NC1. TFAA shows two bands in this region, centered at 1877 and 1813 cm^{-1}, which correspond to the asymmetric and symmetric stretching modes fore each of the two C═O bonds in the anhydride functional group of TFAA, respectively.[51] Electronic coupling of these two stretching modes results in a well-characterized band separation of 60−70 cm^{-1}.[51] After exposure of NC1 to TFAA (Figure 9c), however, only a single band is observed at 1785 cm^{-1} in the carbonyl stretching region. PTFA also exhibits only one band at 1799 cm^{-1} in the carbonyl stretching region. The fact that the derivatized NC1 and PTFA both exhibit a single peak at similar frequencies supports the idea that the exposure of NC1 to TFAA leads to derivatization of the hydroxyl groups on NC1.

(51) Redington, R. L.; Lin, K. C. *Spectrochim. Acta A* **1971**, *27*, 2445.

Analysis of the C−F stretching frequency region (dotted box in Figure 9) provides additional confirmation that TFAA derivatizes hydroxyl groups on NC1. Specifically, Figure 9c shows that, after reaction with TFAA, there is a band in the derivatized NC1 spectra centered at 1150 cm^{-1}, along with a shoulder at 1200 cm^{-1}. These band positions, as well as the overall C−F spectral envelope, are qualitatively similar to those of the C−F stretching modes in PTFA, which exhibits bands at 1125 and 1162 cm^{-1} (Figures 9b and 9c). In contrast, the C−F stretching modes associated with the parent TFAA molecule are located at 1235, 1176, and 1029 cm^{-1} (Figure 9a).[51]

The absence of any spectroscopic IR signature associated with TFAA also supports the conclusion from XPS analysis that TFAA does not physisorb on the extended graphene sheets of BC materials. Therefore, the only F(1s) XPS signal observed after exposing BC materials to TFAA can be attributed to reaction 1.

3.3.3. Comparison of Bulk and Surface Oxides on BC Materials. Another implication of Figure 9 is that the chemical derivatization reactions employed in this study are not restricted to the uppermost surface atoms probed by XPS, but also occur in the bulk of the BC material (ATR-IR probes the uppermost 1 μm of the material).[52] The diffusion and subsequent reaction of the derivatizing agents below the very topmost surface layers can be ascribed to the porosity of the BC materials coupled with the relatively small size of the derivatizing agents.

To provide a semiquantitative measure of the oxide concentrations within the bulk of BC materials, a limited number of EDS studies were carried out on derivatized BC samples. These data were then compared to the corresponding surface oxide concentrations obtained from XPS. In contrast to XPS, EDS is a bulk sensitive technique, which provides information on the elemental composition within the uppermost 5 μm of a sample.[52] A comparison of the O/C ratios obtained from XPS and EDS analysis of NC1 and DS illustrates that the oxygen content decreases significantly in the bulk of both BC materials compared to the surface. For example, the O/C ratios of NC1 and DS are 0.21 and 0.10 as determined by EDS, while XPS analysis of the same samples yields values of 0.30 and 0.20, respectively. The concentration gradient observed upon moving from the surface to the bulk of the NC1 is probably a consequence of the fact that the surface of the BC material experiences the highest local concentration of oxygen and water vapor both during and after the combustion process.

Figure 10 shows a comparison of the surface and bulk concentrations of hydroxyl, carboxylic acid, and carbonyl groups detected on NC1 and DS. These values were determined from the F(1s) signal observed from XPS and EDS measurements after derivatization experiments. In general, the concentration of each surface oxide decreases within the bulk of the sample. For example, Figure 10 shows that on NC1 the hydroxyl and carbonyl groups are present at significantly higher concentrations on the surface than in

(52) Skoog, D. A.; Holler, F. J.; Nieman, T. A. *Principles of Instrumental Analysis*, Fifth ed.; Harcourt Brace College Publishers: New York, 1998.

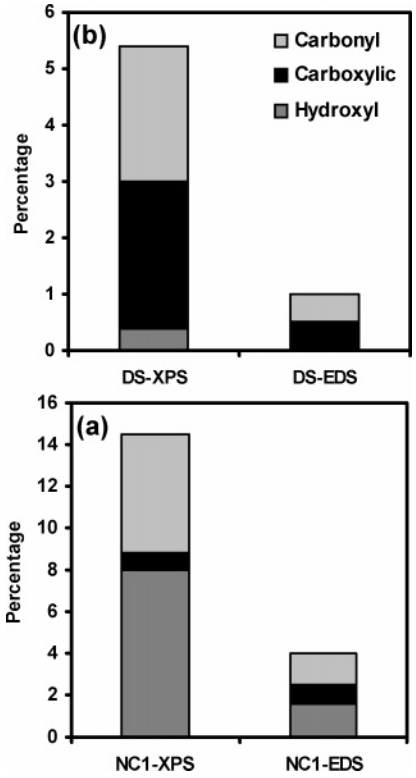

Figure 10. Derivatization results for hydroxyl, carboxylic acid, and carbonyl functional groups on the surface (XPS) and in the bulk (EDS) of NC1(a) and DS(b).

the bulk. In certain cases, however, there appears to be relatively little change in the concentration of a specific oxide within the bulk of the sample compared to that on the surface. One example is the concentration of carboxylic acid groups on NC1. It should be noted, however, that the lack of control experiments analogous to those described for XPS and the potential role of diffusion in limiting the extent of derivatization occurring within the bulk of the BC means that EDS results must be treated on a more qualitative basis.

IV. Potential Applications

The methodology developed in this study can be used in a number of scientifically and technologically important situations that involve carbonaceous materials. For example, different oxidation strategies (e.g., H_2O_2 and ozonolysis) are often used to improve the adsorptive capacities of activated carbons toward specific environmental contaminants.[8,9,13,53,54] Currently, these treatment strategies are developed on a "trial and error" basis, in large part due to the fact that the changes in the surface chemistry that accompany oxidation cannot be easily identified and/or quantified. The methodology developed in this study offers the potential to isolate dominant surface structure−activity relationships for a number of important sorption processes, and thus improve the efficiency of selected sorption strategies.

In addition to BCs the methodology developed in this study could also be applied to other environmental particulates. Specifically, these strategies could be used to determine the concentration of phenolic and carboxylic acid functional groups on the surface of natural organic matter (NOM). These two functional groups are widely recognized to be the dominant oxides on NOM and play a crucial role in governing the chemical properties and solubility of NOM.[55]

Applications of this approach are not limited to environmentally relevant materials. For example, the methods described in this investigation could also be applied to quantify the oxide concentrations on sputter-deposited amorphous carbonaceous films and carbon nanotubes. Oxides play an important role in determining the overall chemical and physical properties of these advanced materials.

Acknowledgment. Professor William, P. Ball and Dr. Thanh H. Nguyen are thanked for helpful discussions and comments, as well as Professor Dwight Smith for providing the DS. The authors would also like to thank Mark Koontz for assistance with acquisition of the EDS data, the Materials Science Department at JHU for use of the surface analysis laboratory, and Professor Gerald J. Meyer for the use of his spin coater. This work was funded by the National Science Foundation (BES # 0332160).

Supporting Information Available: Five additional figures. This material is available free of charge via the Internet at http://pubs.acs.org.

CM051462K

(53) Gomez-Serrano, V.; Acedoramos, M.; Lopez-Peinado, A. J.; Valenzuela-Calahorro, C. *Fuel* **1994**, *73*, 387.
(54) Krishnankutty, N.; Vannice, M. A. *Chem. Mater.* **1995**, *7*, 754.
(55) Chi, F.; Amy, G. L. *J. Colloid Interface Sci.* **2004**, *274*, 380.